Journal of Materials Chemistry A

PAPER

View Article Online
View Journal | View Issue

Check for updates

Cite this: J. Mater. Chem. A, 2017, 5, 12889

Design of salt–metal organic framework composites for seasonal heat storage applications†

Anastasia Permyakova,[ab] Sujing Wang,[a] Emilie Courbon,[b] Farid Nouar,[ac] Nicolas Heymans,[b] Pierre D'Ans,[d] Nicolas Barrier,[e] Pierre Billemont,[b] Guy De Weireld,[b] Nathalie Steunou,*[a] Marc Frère*[b] and Christian Serre*[ac]

Porous materials are recognized as very promising materials for water-sorption-based energy storage and transformation. This study presents the first attempt to use Metal Organic Frameworks (MOFs) as host matrices of salts for the preparation of composite sorbents for seasonal heat storage. We have considered six water stable MOFs (*i.e.* MIL-127(Fe), MIL-100(Fe), MIL-101(Cr), UiO-66(Zr)–NH_2, MIL-125(Ti)–NH_2 and MIL-160(Al)) differing in their crystalline structure, hydrophilic–hydrophobic balance, pore size/shape and pore volume. The successful encapsulation of $CaCl_2$ in the pores of MOFs leads to two series of MOFs–$CaCl_2$ composites whose salt content could be finely tuned depending on the pore volume of MOFs and the synthesis conditions. These materials were fully characterized by combining multiple techniques (*i.e.* powder X-ray diffraction, thermogravimetric analysis, scanning electron microscopy, X-ray energy-dispersive spectrometry elemental mapping, N_2 sorption and elemental analysis). The water sorption properties of these composites were studied under conditions of a solar heat storage system (*i.e.* adsorption at 30 °C, desorption at 80 °C, both steps at a water vapour pressure of 12.5 mbar) in comparison to the parent MOFs. We analyze how the physico-chemical and structural properties of these host matrices impact the energy density of composite sorbents. We show that two mesoporous MOFs–$CaCl_2$ composites (*i.e.* MIL-100(Fe)/$CaCl_2$ and MIL-101(Cr)/$CaCl_2$) with the highest salt loading (46 and 62 wt% respectively) exhibit very high energy storage capacities (up to 310 kW h m^{-3} (485 W h kg^{-1})) outperforming the best composites or physical sorbents reported so far together with very little loss upon adsorption–desorption cycling and high chemical stability upon ageing (up to 18 months).

Received 8th April 2017
Accepted 18th May 2017

DOI: 10.1039/c7ta03069j

rsc.li/materials-a

Published on 18 May 2017. Downloaded on 30/06/2017 09:17:27.

Introduction

Nowadays, the increasingly austere problems of excessive fossil fuel consumption and greenhouse gas emissions produced by combustion processes are encouraging the development of efficient and affordable alternative energy solutions. Thermochemical energy storage, based on reversible reactions involving working fluids, is a very efficient way of heat reallocation with extremely low losses, and tunable cycle times, from months for seasonal applications to minutes for heat transformation, heat pumping or refrigeration applications (see Fig. S1 for more information†). So far, only heat pumping and refrigeration applications are mature and water is the most widespread working fluid used due to its high evaporation enthalpy (*i.e.* 2500 kJ kg^{-1} at 1 bar and 373 K), non-toxicity and availability.[1–3] Water is also considered to be an interesting working fluid for potential seasonal storage applications mainly due to its lack of toxicity. For all these applications, hydrothermally stable and scalable materials with a high energy density or energy capacity (especially for seasonal storage applications), fast kinetics of adsorption (particularly for heat transformation, heat pumping and cooling applications), and stability under numerous adsorption–desorption cycles are required.[1–3] Moreover, the water sorption characteristics of materials have to match the operating conditions of each application.[1–3] In the case of closed system configurations, these operating conditions are defined by the temperatures of (i) the cycle boundary of water evaporation (T_e), (ii) condensation (T_c) and (iii) regeneration. For heat

[a]Institut Lavoisier, UMR CNRS 8180, Université de Versailles St-Quentin en Yvelines, Université Paris-Saclay, 45 Avenue des Etats-Unis, 78035 Versailles Cedex, France. E-mail: nathalie.steunou@uvsq.fr

[b]Institut de Recherche en Energie, Service de Thermodynamique et de Physique mathématique, Université de Mons, Boulevard Dolez 31, B-7000 Mons, Belgium. E-mail: marc.frere@umons.ac.be

[c]Institut des Matériaux Poreux de Paris, FRE 2000 CNRS, Ecole Normale Supérieure, Ecole Supérieure de Physique et des Chimie Industrielles de Paris, PSL Research University, 75005 Paris, France. E-mail: christian.serre@ens.fr

[d]4MAT Department, Université libre de Bruxelles (ULB), 50 Avenue F. D. Roosevelt – CP 194/3, B-1050 Bruxelles, Belgium

[e]Laboratoire CRISMAT, CNRS UMR 6508, 6 bvd Maréchal Juin, 14050 Caen Cedex, France

† Electronic supplementary information (ESI) available: Fig. S1–S71 and Tables S1–S4. See DOI: 10.1039/c7ta03069j

Published on 18 May 2017. Downloaded on 30/06/2017 09:17:27.

pumping applications, the materials should present a high water uptake (*i.e.* cycling loading lift) at a typical relative working pressure p/p_0 below 0.3 (depending on the process temperature).[1–3] For seasonal heat storage applications, high quantities of energy have to be handled in one cycle so that high values of the cycling loading lift enable a reasonable size of the storage system.[4–6]

Inorganic porous materials have been investigated for such applications, due to their fast kinetics of water sorption typical of pure physical adsorbents.[7] While silica gels can be regenerated at very low temperatures (down to 45–50 °C), they exhibit typically a low water sorption capacity, within the 0.03–0.10 g g^{-1} range for a typical adsorption heat pump (AHT).[8] Due to their high hydrophilic character, zeolites present a large water sorption uptake at quite low values of the relative pressure, but high regeneration temperatures are required (over 140 °C).[1–3] Aluminophosphates (AlPOs) and silica-aluminophosphates (SAPOs) were also considered, however with limited interest for seasonal storage due to their high cost and low water adsorption capacity,[3,9] except for a few recently developed candidates.[10,11] Inorganic porous materials exhibit on the whole energy outputs of 50–100 kW h m^{-3} [2] which is considered as too low for seasonal storage applications. In contrast, chemical sorption materials, such as hygroscopic salts, exhibit the highest energy output (up to ~600 kW h m^{-3}) which is highly suitable for seasonal storage applications, but at the expense of very slow water sorption kinetics.[4,5,12] In addition, due to the hygroscopic character and possible redissolution of salts upon water sorption, their poor stability under multiple adsorption–desorption cycles remains the key issue for their practical use.[12–14] Therefore, the design of composite materials (an inorganic salt confined in a porous host matrix) was reported as a promising approach. Indeed, a synergy between the physical sorption of the host matrix and the chemical sorption of the salt as well as the possible absorption of water vapour by superconcentrated salt solution may be expected.[15–17] In composites, the behaviour of individual components (inorganic salt and porous matrix) may be significantly modified in terms of water sorption properties, kinetics, packing density, stability and regeneration temperature. In particular, the sorption properties of composites can be tuned by varying the chemical nature, loading capacity and particle size of the confined salt and depend strongly on the microstructural and physico-chemical properties of the porous host matrix (pore size, shape and volume, and hydrophilic–hydrophobic balance).[18–22]

Metal–organic frameworks (MOFs) represent a recent class of crystalline hybrid porous materials obtained by assembling metal nodes and organic ligands. One can easily tune their structural and chemical features due to the large variety of possible metal cations and organic linkers and their almost infinite number of combinations. Thus, due to their micro- or mesoporous character, their surface area values lie typically between a few hundred and thousands of m^2 g^{-1}, exceeding in most cases the values of "usual" porous materials.[23] As a result of their fascinating physico-chemical properties, these materials present potential applications in gas storage/separation,[24,25] catalysis,[26–29] biomedicine,[30,31] and sensing,[32–34] among others. Recently, this class of crystalline hybrid materials has emerged as promising water sorption materials for heat transformation.[1,3,35–43] In particular, a series of MILs (MIL stands for Material from Institut Lavoisier) or UiOs (UiO stands for Material from University of Oslo) that comprised of three- and four-valent metal cations (Cr^{3+}, Al^{3+}, Fe^{3+}, Zr^{4+} and Ti^{4+}) and aromatic polycarboxylate linkers (see Fig. 1) were considered for water sorption applications.[1,35,38,44–50]

These materials (*i.e.* MIL-127(Fe),[51] MIL-100(Fe, Al, Cr),[27] MIL-101(Cr),[52] UiO-66(Zr)–NH_2,[53,54] MIL-125(Ti)–NH_2,[55] and MIL-160(Al)[44]) all exhibit a good hydrothermal stability, water adsorption isotherms with a "S" shape profile, low regeneration temperatures and total water uptake ranging from 0.5 to 1.5 g g^{-1} particularly suitable for heat reallocation applications (see ESI†).[35,38,44–46,50,56] In addition, the use of hydrophilic amino groups from the organic ligand or the presence of hydroxo groups from the inorganic node enables the tuning of their sorption behaviour in terms of water uptake (*i.e.* adsorption loading lift) as well as their hydrophilic character (position of step in p/p_0). Very recently, composites based on $CaCl_2$ and UIO-66(Zr) (or its NH_2 functionalized analog, UIO-66(Zr)–NH_2) were considered for adsorption thermal battery or chiller applications with interesting properties in terms of heat storage capacity (*i.e.* 367 kJ kg^{-1}), specific cooling power (*i.e.* 631 W kg^{-1}) and cycling stability.[57]

The present paper deals with the first attempt to consider this series of stable MOFs as host matrices of salts for the preparation of composite sorbents for seasonal heat storage. This is to analyse how the physico-chemical and structural properties of MOFs will impact the energy density of composite sorbents. One expects first that the position of the adsorption loading lift (p/p_0) in composites might strongly depend on the pore size of the host matrix.[2,20] Another critical issue here concerns the chemical and thermodynamic compatibility between MOFs and salts as the stability and water sorption properties of composites strongly depend on the interfacial

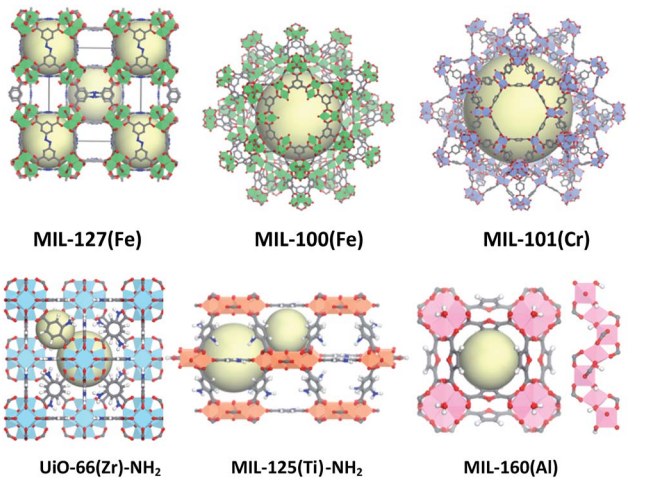

Fig. 1 Polyhedral representation of MOFs. The cavity space is indicated by yellow van der Waals spheres (Fe, green; Cr, purple; Zr, blue; Ti, orange; Al, pink; C, gray; N, blue; O, red; and H, white).

 This journal is © The Royal Society of Chemistry 2017

Published on 18 May 2017. Downloaded on 30/06/2017 09:17:27.

properties between the porous matrix and the salt while this governs both the salt dispersion/aggregation and the free pore volume of the sorbent. A series of MOF based composites with high $CaCl_2$ content was prepared with high energy storage capacity. Moreover, we show that two mesoporous MOFs–$CaCl_2$ composites with the highest salt loading exhibit very high energy storage capacities (up to 310 kW h m^{-3} (485 W h kg^{-1})) outperforming the best composites or physical sorbents reported so far together with very little loss upon cycling and high chemical stability upon ageing.

Experimental section

Synthesis of salt–MOF composites

The MOF sample was dried for 3 hours in an oven at 100 °C, before one encapsulation step using $CaCl_2$ solution with a soaking time of 2 hours. The sample was collected following the removal of excessive $CaCl_2$ solution by centrifugation and was completely dried at 100 °C in an oven overnight. For more details, see the ESI.†

Characterization of materials

Powder X-ray diffraction patterns of MOFs were obtained on a Siemens D5000 diffractometer using CuK$\alpha_{1,2}$ radiation (λ = 1.5406 Å) within the 0.2–60° 2θ range, with a step of 0.02°. Powder X-ray diffraction patterns of salt–MOF composites were recorded on a Bruker D8 Advance Vario1 diffractometer using pure CuKα1 radiation (λ = 1.540598 Å) and equipped with an Anton Paar HTK1200N high temperature chamber. The PXRD diagrams were collected at 25 °C and 150 °C between 3 and 60°(2θ) with a step of ~0.009°(2θ). The BET surface area was calculated from N_2 adsorption–desorption isotherms measured on a Belsorp Mini (Bel, Japan) at liquid nitrogen temperature (77 K). Prior to the analysis, samples were dried for 12 h under primary vacuum. The BET surface area and micropore volume were estimated at a relative pressure below 0.25. Thermogravimetric (TG) measurements were carried out on a thermogravimetric analyzer (Perkin Elmer Diamond TGA/DTA STA 6000) with an oxygen flow of 200 mL min^{-1}. The temperature was increased from 303 K to 873 K. SEM-EDX analysis was performed using gold-coated samples on a JEOL JSM-7001F microscope equipped with an energy-dispersive X-ray (EDX) spectrometer and an X-Max SDD (Silicon Drift Detector) from Oxford.

Water sorption and calorimetric measurements

The cycling loading lift, multiple cycles of water adsorption–desorption under cycle boundary conditions (a pressure of 12.5 mbar, an adsorption temperature of 30 °C and a desorption temperature of 80 °C) and calorimetric measurements were carried out using a thermogravimetric analyzer (TG-DSC111) connected to a humidity generator (Setaram) with an RH stability of ±0.3%. The sample was first dried for 12 h under vacuum at the same temperature as that for N_2 sorption measurements for each sample. The sample is then put in contact with humid nitrogen (flow rate: 50 mL min^{-1}, bath and gas temperature: 40 °C, and relative humidity: 17.4%) at 30 °C. When equilibrium is reached, the sample is heated to 80 °C at 1 °C min^{-1}, and the desorbed mass and the heat flow signals are simultaneously recorded. The desorbed mass between 30 °C and 80 °C at 12.5 mbar corresponds to the cycling loading lift. The integration of the heat flow signal enables us to obtain the heat of sorption. For further use as the energy storage capacity, this value has to be corrected with the integration of the heat flow signal of a blank test (prior to the measurement, the blank test is done under the same conditions with empty crucibles), and by taking into account the heat required to heat the sample and the water vapour from 30 °C to 80 °C.

For adsorption heat measurements only the adsorption step (T = 30 °C and p = 1.25 kPa) was considered (humidity generator at 40 °C and relative humidity RH = 17.4%). The integration of the heat flow signal using the horizontal last point integration mode gives the heat of adsorption expressed in J g^{-1} of MOF. For more details, see the ESI.†

Results and discussion

Water sorption properties of MOFs under conditions of a solar heat storage system

The sorption properties of MOFs alone (see Fig. S2–S19 of the ESI† for full characterization) have been studied under conditions close to those of the application, in light of their physicochemical characteristics (Table 1). Sorption isotherms or cycling loading lifts were measured under conditions of a seasonal energy storage system (see Fig. S20–S26†). Here, the operating conditions are the following: T_d = 80 °C (desorption temperature typical of a solar collector), T_a = 30 °C (minimum adsorption temperature for space heating during the winter period) while the evaporation and condensation temperatures of 10 °C (T_c and T_e) corresponding to a pressure of 12.5 mbar for a closed system were chosen. For each MOF, the mass change was calculated as gram of water per gram of anhydrous MOF measured between 30 °C and 80 °C at 12.5 mbar for each cycling loading lift. In addition, the mass change at the adsorption step (30 °C at 12.5 mbar) was also evaluated (*i.e.* adsorption loading lift) (see Fig. S20 of the ESI†). Two main parameters have been considered here for the MOFs: (i) their hydrophilic–hydrophobic balance and (ii) their pore size/shape. First, we have considered a series of microporous MOFs bearing a pronounced hydrophilic character, due to a combination of hydroxylated inorganic building units and the polarity of the organic linker: UiO-66(Zr)–NH_2,[54] MIL-125(Ti)–NH_2 [55] or MIL-160(Al) (2,5-furandicarboxylic acid (FDCA)).[44] UiO-66(Zr)–NH_2 and MIL-125(Ti)–NH_2 both exhibit a 3D network made up of two tetrahedral or octahedral cages with pore sizes of 7.5/12 Å and 6/12 Å, respectively. In both structures, the framework is built by connecting metal oxo/hydroxo clusters (*i.e.* $Zr_6O_4(OH)_4$ and $Ti_8O_8(OH)_4$) and terephthalate based linkers.[54,55] In MIL-160(Al) the helical *cis*-corner-sharing chains of $AlO_4(OH)_2$ octahedra are connected *via* carboxylate groups of FDCA resulting in a 1D pore system based on square shaped sinusoidal channels of ~5 Å.[44] As previously reported,[35,44,56] these solids present similar one-step S-shaped isotherms with steep uptake at relative pressure

Table 1 Structural and sorption characteristics of MOFs

MOF	Pore diameter, (Å)	S_{BET} ($m^2\ g^{-1}$)	Total pore volume ($cm^3\ g^{-1}$)	Structural characteristics	Adsorption loading lift at[ab] 30 °C, g g^{-1}	Cycling loading lift[ab], g g^{-1}
MIL-100(Fe)	25/29	1828	0.81	Acid Lewis sites	0.39	0.32
MIL-101(Cr)	29/34	3721	1.51	Acid Lewis sites	0.17	0.12
MIL-127(Fe)	5/7/10	1342	0.57	Acid Lewis sites	0.28	0.20
UiO-66(Zr)–NH_2	7.5/12	1119	0.44	Hydrophilic centres (–NH_2)	0.33	0.32
MIL-125(Ti)–NH_2	6/12	1480	0.64	Hydrophilic centres (–NH_2)	0.39	0.37
MIL-160(Al)	5	1148	0.46	Hydrophilic centres (O-heteroatom)	0.37	0.36

[a] Standard deviations of adsorption and cycling loading lifts are close to 1%. [b] gram of water per gram of dry MOF.

Published on 18 May 2017. Downloaded on 30/06/2017 09:17:27.

p/p_0 = 0.30, 0.25 and 0.20, respectively. In this work, we have shown that for UiO-66(Zr)–NH_2, MIL-125(Ti)–NH_2 and MIL-160(Al) the adsorption loading lifts (T = 30 °C, 12.5 mbar) and cycling loading lifts (12.5 mbar, T_a = 30 °C, T_d = 80 °C) are equal to 0.33 and 0.32 g g^{-1}, 0.39 and 0.37 g g^{-1}, and 0.37 and 0.36 g g^{-1}, respectively (Fig. S21–S23†). In contrast, if one considers the more hydrophobic microporous MIL-127(Fe) and the mesoporous MIL-100(Fe) and MIL-101(Cr) MOFs, a shift of their sorption steps towards higher p/p_0 is observed together with two-step isotherms due to their bimodal pore system.[36,38] These solids are built by oxo-centered trimers of metal octahedra and polycarboxylate ligands (terephthalate for MIL-101(Cr), trimesate for MIL-100(Fe), and 3,3′,5,5′-azobenzenetetracarboxylate for MIL-127(Fe)). MIL-127(Fe) exhibits a microporous cubic structure with a soc topology[51] and its two-step water sorption isotherm can be explained by the consecutive filling of hydrophilic cages (~10 Å) or channels (~5 Å) and then hydrophobic pores (~7 Å) leading to two uptakes at p/p_0 = 0.30 and at p/p_0 = 0.60, respectively (T = 30 °C). MIL-100(Fe) and MIL-101(Cr) present a MTN zeolite topology with two types of mesoporous cages of 24/27 Å and 27/34 Å, respectively,[27,52] high specific surface areas and a high concentration of Lewis acid sites (Table 1). This is associated with step-wise shape water sorption isotherms and large water uptakes.[36,38,46] For MIL-100(Fe), as reported before, two stepwise uptakes of 0.49 g g^{-1} at p/p_0 = 0.35 and 0.35 g g^{-1} at p/p_0 = 0.45 correspond to the consecutive filling of the 25 Å and 29 Å mesoporous cages, respectively.[36,38] Due to its more hydrophobic character, MIL-101(Cr) exhibits a stepwise water uptake close to 1.20 g g^{-1} shifted to a higher relative pressure of p/p_0 = 0.4–0.5, as previously reported,[46,58] with consecutive filling of the two different mesopores of 29 and 34 Å (*i.e.* the first adsorption lift of 0.97 g g^{-1} at p/p_0 = 0.40 and the total adsorption lift of 1.55 g g^{-1} at p/p_0 = 0.50). Despite their rather large pore volumes, the adsorption loading lifts and cycling loading lifts of MIL-127(Fe), MIL-100(Fe) and MIL-101(Cr) are not larger than those of the hydrophilic MOFs with values respectively of 0.28 and 0.20 g g^{-1}, 0.39 and 0.32 g g^{-1}, and 0.17 and 0.12 g g^{-1} (Fig. S20†). In addition, these MOFs exhibit a suitable stability under numerous adsorption–desorption cycles. It has been previously reported that the mass loss of exchanged water is 3.2% (40 cycles), 6.37% (40 cycles), 17% (40 cycles), 38% (40 cycles) and 0% (10 cycles) for respectively MIL-101(Cr), MIL-100(Fe), MIL-125(Ti)–NH_2, UiO-66(Zr)–NH_2 and MIL-160(Al).[35,36,44,58] This series of MOFs also shows great promise for such applications due to the possibility to easily scale up their synthesis on a laboratory scale.[59] Moreover, MIL-100(Fe)[60] and MIL-101(Cr)[52] can be synthesized using H_2O as the solvent, MIL-127(Fe)[51] in alcohols while MIL-160(Al)[44] is obtained through a green route using a bio-derived linker.

Synthesis and characterization of MOFs–$CaCl_2$ composites

In the second step, composites combining MOF matrices and $CaCl_2$ were prepared. Calcium chloride was selected due to its large availability, low cost and hydration rate (*i.e.* 5 moles of water per mole of $CaCl_2$) under conditions of thermochemical storage for space heating (*i.e.* adsorption at 30 °C, desorption at 80 °C, vapour pressure between 872 and 1704 Pa). The MOFs were dried for 3 hours in an oven at 100 °C, followed by impregnation of aqueous solutions of $CaCl_2$ of different concentrations (see the ESI for details on the synthesis of composites and Table S1†). The influence of the soaking time, sample washing, concentration of $CaCl_2$, temperature, and number of encapsulation steps on the microstructural properties and composition of composites was investigated. Washing of composites with H_2O or EtOH initially, to remove the excess of salt at the outer surface of MOF particles, was ruled out due to the excessive removal of the salt initially encapsulated. The temperature during the encapsulation process was fixed to ambient values since higher temperatures led to unstable composites with a large amount of salt located at the outer surface of MOF particles. Two methods of encapsulation were studied. In the first one, each encapsulation step was followed by centrifugation and removal of the liquid phase with, however, a negligible increase of the salt content with the number of encapsulation steps. The second method required a drying of the composites after each encapsulation step which led to an enhancement of the salt content but also to a partial recrystallization of the salt at the surface of MOF particles. Finally, we selected the one-step encapsulation procedure and modulated the concentration of the initial salt solution to tune the salt content in the composites with homogeneously distributed salt in a reproducible manner. Finally, composites with a $CaCl_2$ content varying between 30 and 62 wt% were

 This journal is © The Royal Society of Chemistry 2017

Published on 18 May 2017. Downloaded on 30/06/2017 09:17:27.

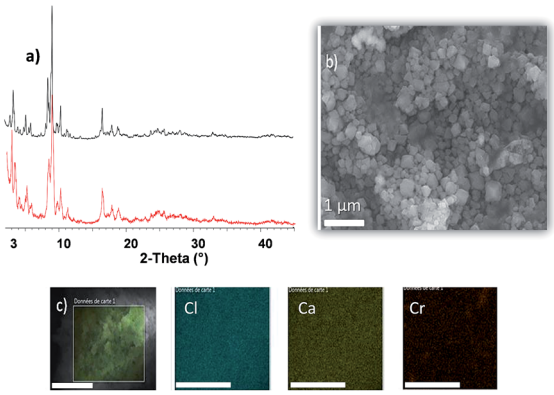

Fig. 2 Characterization of MIL-101(Cr)/$CaCl_2$ (62 wt%). (a) PXRD diagram of MIL-101(Cr)/$CaCl_2$ (62 wt%) (red) obtained after washing with water in comparison with that of MIL-101(Cr) (black); (b) SEM image; and (c) elemental XEDS mapping area images. The scale bar corresponds to 5 µm.

obtained and fully characterized through a combination of powder X-ray diffraction (PXRD), thermogravimetric analysis (TGA), scanning electron microscopy (SEM), X-ray energy-dispersive spectrometry (XEDS) elemental mapping, N_2 sorption and elemental analysis (see Fig. 2 and S27–S60 of the ESI†).

Powder X-ray diffraction (PXRD) patterns of the composites were collected at room temperature and 150 °C. Firstly, for the whole series of composites, the X-ray diffraction patterns are in good agreement with those of pure MOFs indicating that the structure of MOFs is preserved in the composites (see Fig. 2 and S27–S36†). Secondly, for the composites with the highest salt rate (*i.e.* MIL-127(Fe)/$CaCl_2$ (40 wt%)), the presence of recrystallized $CaCl_2 \cdot 2H_2O$ (25 °C) or anhydrous $CaCl_2$ at 150 °C is clearly evidenced and is likely to be due to the recrystallization of a small amount of salt at the outer surface of MOF particles (Fig. S28†). Finally, in the case of composites based on large pore MIL-100(Fe) and MIL-101(Cr), a significant decrease of the relative intensity of the diffraction Bragg peaks is observed at room temperature and 150 °C, especially at low angles, which is probably due to both a modification of the electronic density (and thus a strong absorbance of the X-ray by the materials) and the strongly disordered hydrated salt within the mesoporous cages.[60] To prove such an assumption, we carried out a similar PXRD analysis using the same samples but they were washed with water to remove the salt. It is noteworthy that the PXRD patterns after washing with water are similar to those of the parent MOFs (see Fig. 2 and S35 and S36†) confirming the preservation of their structure after the salt loading. In addition, the SEM images of the composites show that the morphology of MOF crystallites is not altered after the salt encapsulation (see Fig. 2 and S45–S52†). The salt rates determined by thermogravimetric analysis, XEDS analysis and elemental analysis (see Table S2†) are in good agreement. According to SEM and XEDS elemental mapping, no $CaCl_2$ crystallites can be observed in the samples, either at the surface of MOF particles or in the interparticle space.

The calcium/metal (Ca/metal) ratios measured by XEDS (Table S2†) are on the whole similar for 3 areas of each composite, confirming the homogeneous distribution of the salt among the different MOF particles, although in the case of UiO-66(Zr)–NH_2/$CaCl_2$ (43 wt%) and MIL-125(Ti)–NH_2/$CaCl_2$ (45 wt%), a slightly more heterogeneous Ca/Me ratio may arise from a larger particle size distribution, thereby affecting the diffusion and location of the salt. Nevertheless, for all MOF based composites, the total salt content for each composite is comparable (see Table S2†). Nitrogen sorption isotherms of the composites show as expected a strong decrease of the pore volume and BET surface area as a result of the salt entrapment (see Fig. S53–S60 of the ESI†). It is noteworthy that depending on both the salt content and the type of MOF, a residual porosity remains after salt incorporation and may contribute to the water adsorption of the composites.

In order to shed light on the influence of $CaCl_2$ content on the water sorption properties of composites, two series of MOFs–$CaCl_2$ composites with different salt contents were further prepared: (i) a first one with a similar salt content, *i.e.* close to 31–34 wt%, and (ii) a second series with an increased salt loading between 40 and 62 wt%. The analysis of the first series of composites highlighted the impact of the water physical sorption in MOFs on the water uptake of composites, in direct relationship with the hydrophilic character and the free pore volume of the MOFs. The second series, which includes composites with higher salt contents, shows the effect of their amphiphilic character, residual pore volume and salt loading capacity on the water uptake. It is noteworthy that for each MOF structure and considering their theoretical pore volume, it was possible to estimate an upper limit range of salt content to be encapsulated assuming the total filling of the pores by $CaCl_2$ tetrahydrate or hexahydrate (see Table 2). However, one could point out that these values might be slightly overestimated since one could expect that not all of the pore volume is accessible to such a bulky salt. For instance, MIL-127(Fe) exhibits two types of porosities: 1-D channel systems (~5–8 Å) and larger cages (~10 Å) with very narrow windows (~3 Å) and thus not accessible to the salt. Thus, a complete pore filling by the salt is impossible for this MOF and as a consequence the experimental loading capacity in MIL-127(Fe) shall be significantly lower than 48 wt%. Only in the case of UiO-66(Zr)–NH_2/$CaCl_2$ (43 wt%), the experimental result slightly exceeds the theoretical one, with no evidence of recrystallized salt detected by PXRD (see Fig. S29†), which is probably due to the presence of linker defects leading to a larger pore volume of the sample.[61] It is noteworthy that, as expected, increasing the pore volume through the use of mesoporous MOFs such as MIL-100(Fe) (1.02 $cm^3\ g^{-1}$ theor.) and MIL-101(Cr) (1.95 $cm^3\ g^{-1}$ theor.) leads to higher salt loadings (*i.e.* 46 and 62 wt%), far beyond the values obtained with composites based on silica gel (28–34 wt%).[62,63]

Water sorption properties of MOFs–$CaCl_2$ composites with low salt content (31–34 wt%) under conditions of a solar heat storage system

The water sorption behaviour of the first series of composites with similar salt contents (31–34 wt%) was studied under conditions of a seasonal energy storage system (see the above-

Published on 18 May 2017. Downloaded on 30/06/2017 09:17:27.

Table 2 Properties of the MOF–salt composites

MOF	$CaCl_2$ content[a] (%, wt)	Upper limit range of $CaCl_2$[b] (%, wt)	Total pore volume of MOF (theor.) ($cm^3\ g^{-1}$)	S_{BET} of composite[c] ($m^2\ g^{-1}$)	Total pore volume of composite[c] ($cm^3\ g^{-1}$)	Adsorption lift[d], $g\ g^{-1}$	Cycling lift[d], $g\ g^{-1}$	Energy storage capacity[f] Calc. ($W\ h\ kg^{-1}$)	Energy storage capacity[f] Exp. ($W\ h\ kg^{-1}$)
MIL-160(Al)	34	27–36	0.50	520 ± 20	0.240 ± 0.006	0.35 ± 0.01[e]	0.21 ± 0.01[e]	—	—
UiO-66(Zr)–NH_2	43	27–36	0.50	310 ± 10	0.130 ± 0.004	0.47 ± 0.02[e]	0.33 ± 0.02[e]	248	268 ± 50[e]
MIL-125(Ti)–NH_2	45	35–46	0.78	360 ± 20	0.240 ± 0.004	0.46 ± 0.02[c]	0.35 ± 0.02[c]	254	243 ± 8[c]
MIL-127(Fe)	31	38–48	0.83	520 ± 20	0.228 ± 0.009	0.43 ± 0.03[c]	0.31 ± 0.02[c]	—	—
MIL-127(Fe)	40	38–48	0.83	520 ± 10	0.223 ± 0.005	0.43 ± 0.02[e]	0.33 ± 0.02[e]	243	228 ± 20[e]
MIL-100(Fe)	34	43–53	1.02	370 ± 50	0.188 ± 0.005	0.45 ± 0.01[c]	0.32 ± 0.01[c]	—	—
MIL-100(Fe)	46	43–53	1.02	290 ± 20	0.130 ± 0.020	0.57 ± 0.02[c]	0.47 ± 0.02[c]	347	335 ± 20[c]
MIL-101(Cr)	62	59–68	1.95	330 ± 10	0.170 ± 0.010	0.75 ± 0.01[c]	0.58 ± 0.01[c]	428	485 ± 50[c]

[a] Salt content is presented according to chemical analysis. [b] Calculated assuming that the pore volume of MOFs is occupied by the tetrahydrate or the hexahydrate form of $CaCl_2$. [c] Standard error on 3 measurements. [d] Gram of water per gram of dry composite. [e] Standard error on 2 measurements. [f] Energy storage capacity is based on the 1st adsorption cycle without taking into account the decrease of capacity after cycling.

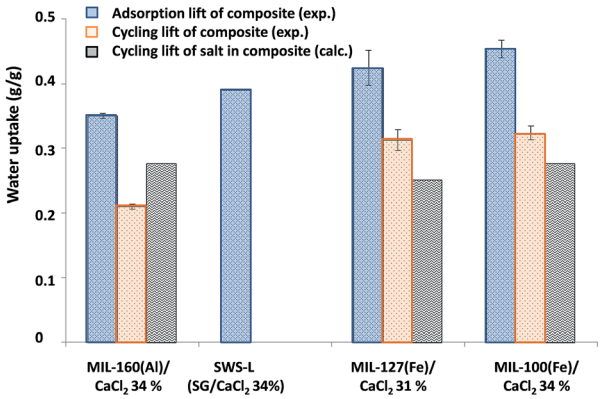

Fig. 3 Adsorption and cycling loading lifts (gram of water per gram of dry composites) of MOF based composites with $CaCl_2$ (31–34 wt%); calculated cycling lift of the salt in the composites and adsorption lift of the SWS-1L composite (silica gel/$CaCl_2$ 34 wt%).[63] Conditions of adsorption lift: 30 °C, $p = 12.5$ mbar (for MOF based composites) and 30 °C, $p = 12.3$ mbar (for SWS-1L). Conditions of cycling lift: adsorption at 30 °C and $p = 12.5$ mbar, and desorption at 80 °C and $p = 12.5$ mbar.

mentioned cycling loading lift conditions) (Fig. 3). For the sake of comparison, we consider these results in light of those of silica gel based composites (*i.e.* SWS-1L) with a 33.7 wt% $CaCl_2$ loading.[63] In addition, for each composite, the cycling loading lift of the bulk salt is calculated by considering the same salt content as that in the composite and its hydration at 12.5 mbar between 30 °C and 80 °C from the monohydrate form to the hexahydrate form (NB: this corresponds to the mass of water theoretically exchanged by an amount of salt encapsulated in each composite under cycling conditions per mass of dry composite). Such a comparison may be useful to show the impact of the physical sorption of MOFs on the water sorption behaviour of composites. The adsorption and cycling loading lifts of the composites (see Fig. S61–S67 of the ESI†) are finally compared to those of pure MOFs (mass of water/mass of dry MOF) (see Table 1). One can first notice that the water uptake of the composites is not improved when dealing with hydrophilic host matrices (see Fig. 3). For instance, for the most hydrophilic MOF in play here, MIL-160(Al), a significantly lower performance was observed compared with those of composites based on more hydrophobic MOFs (*i.e.* MIL-127(Fe) and MIL-100(Fe)). Noteworthily, it is striking for MIL-160(Al) that (i) no improvement in water uptake is evidenced upon salt encapsulation: 0.35 g g^{-1} *versus* 0.37 g g^{-1} for the pure MOF (Table 1) and (ii) the cycling loading lift of the composite is even lower (0.21 g g^{-1}) than that of pure MIL-160(Al) (0.36 g g^{-1}) (Table 1). Such a phenomenon may arise from the very high hydrophilic character of the MIL-160(Al)/$CaCl_2$ composite (34 wt%) due to the polar framework and adsorbed guests (salt and water), leading to a much lower desorption efficiency at 80 °C. Moreover, the desorption of water and thus the complete transition of the salt from the hexahydrate to the monohydrate state may be here strongly hampered by the very slow diffusion of water inside the 1D pore system of MIL-160(Al) whose salt content is close to the upper limit salt content of this MOF. In contrast, when dealing with amphiphilic MOF based composites, *i.e.* MIL-127(Fe)/$CaCl_2$ (31 wt%) and MIL-100(Fe)/$CaCl_2$ (34 wt%), the adsorption and cycling loading lifts are enhanced compared to those of the pure MOFs. Moreover, the experimental cycling lifts of these composites whose salt content is lower than the upper salt limit range are also superior than those calculated for the pure bulk salt (see Fig. 3), as a result of a beneficial synergy between the chemical sorption of the salt and the physical sorption of the MOFs (see Table 2).

Water sorption properties of MOFs–$CaCl_2$ composites with high salt content (>30 wt%) under conditions of a solar heat storage system

To gain further understanding, the second series of composites with larger salt loadings (>30 wt%), *i.e.* MIL-125(Ti)–NH_2/$CaCl_2$ (45 wt%), UiO-66(Zr)–NH_2/$CaCl_2$ (43 wt%), MIL-127(Fe)/$CaCl_2$ (40 wt%), MIL-100(Fe)/$CaCl_2$ (46 wt%) and MIL-101(Cr)/$CaCl_2$ (62 wt%), was evaluated for this application. The amount of $CaCl_2$ is here directly linked to the pore volume of MOFs: the higher the pore volume of MOFs, the higher is the $CaCl_2$ amount encapsulated. Furthermore, the cycling loading lift

 This journal is © The Royal Society of Chemistry 2017

Published on 18 May 2017. Downloaded on 30/06/2017 09:17:27.

increases strongly with increasing salt content as shown by comparing the values of composites with 40–46 wt% $CaCl_2$ and 62 wt% MIL-101(Cr)/$CaCl_2$ (Fig. 4) as well as those of both MIL-100(Fe)/$CaCl_2$ composites with 34 and 46 wt% $CaCl_2$ (Fig. 3 and 4). As observed for the first series of composites, lower cycling loading lift values are typically observed for hydrophilic MOF based composites (*i.e.* MIL-125(Ti)–NH_2/$CaCl_2$ (45 wt%) and UiO-66(Zr)–NH_2/$CaCl_2$ (43 wt%)) or composites with the lowest amount of salt (*i.e.* MIL-127(Fe)/$CaCl_2$ (40 wt%)) (see Fig. 4). Once again, the cycling loading lifts of the composites were compared to those derived by the hydration process of the bulk salt. It is remarkable that for amphiphilic MOF based composites, the cycling loading lift of the composites is larger than that of the pure salt, showing that the water uptake of composites results from a complex interplay between the amphiphilic balance, the residual pore volume of MOFs and the content and location of the salt. In particular, the more hydrophobic character of MOFs may facilitate the desorption process while their residual pore volume may enhance the adsorption process. For instance the MIL-101(Cr)/$CaCl_2$ (62 wt%) composite, which exhibits, to our knowledge, the best performance so far in the field of $CaCl_2$ based porous solid composites, illustrates the ideal structural and physico-chemical requirements for seasonal heat storage applications. This material combines a huge salt content, a moderate hydrophilic character and a significant residual accessible pore volume. Moreover, the 3D mesoporous pore system of MIL-101(Cr) may also promote fast water sorption diffusivity.

Energy storage performance of MOFs–$CaCl_2$ composites with high salt content (>30 wt%)

In the last step, the energy storage capacity of this second series of salt–MOF composites was evaluated, either experimentally through microcalorimetric measurements (experimental energy storage capacity) or calculated by combining data of the cycling loading lift and heat of adsorption (calculated energy storage capacity) (see Fig. 4; Table S3†). Details concerning the calculation and the measurement of energy storage capacities are provided in the ESI.† It is noteworthy that the calculation of energy storage capacities requires the measurement of the heat of water sorption of each MOF. First, one can point out that the experimental and calculated energy storage capacities of the composites are fully consistent (see Fig. 5; Tables 2 and S3 and S4†). The slight discrepancy might arise from the calculation method that does not take into account the complexity of the adsorption phenomenon in salt–MOF composites that involves the hydration of the salt, the physical sorption by the MOF and the interaction between the MOF and the salt. For the two most promising composites, MIL-100(Fe)/$CaCl_2$ (46 wt%) and MIL-101(Cr)/$CaCl_2$ (62 wt%), the experimental energy storage density (kW h m^{-3}) was evaluated based on the experimental energy storage capacity (W h kg^{-1}) by taking into account the packing density of the composites in their powdered forms (see Table S4†). The values for MIL-100(Fe)/$CaCl_2$ (46 wt%) and MIL-101(Cr)/$CaCl_2$ (62 wt%) correspond to 208 kW h m^{-3} (335 W h kg^{-1}) and 310 kW h m^{-3} (485 W h kg^{-1}), respectively. Although the shaping and packing of these MOFs–$CaCl_2$ composites have not been optimized yet, their performances are higher or comparable to those of the most promising composites reported in the literature so far (see Table 3).[64–70] However, we need to keep in mind that any direct comparison of energy storage density is risky, because it strongly depends on the cycle boundary conditions. For example, the increase of desorption temperature from 80 °C to 100 °C will enhance the cycling loading lift and thus the energy storage density. Nevertheless, the state of the art of composite materials developed for space heating applications is shown in Table 3. By considering desorption temperatures lower than 100 °C, the energy storage capacity values of such reported materials ($CaCl_2$ or LiCl encapsulated in a silica gel matrix) lie within the ~130–280 W h kg^{-1} range which is significantly lower than those of salt–MOF composites. The highest energy storage density was found for the silica gel/$CaCl_2$ composite.[70] This silica gel matrix and MIL-100(Fe) have roughly an equal pore volume (0.81 cm^3 g^{-1}) while

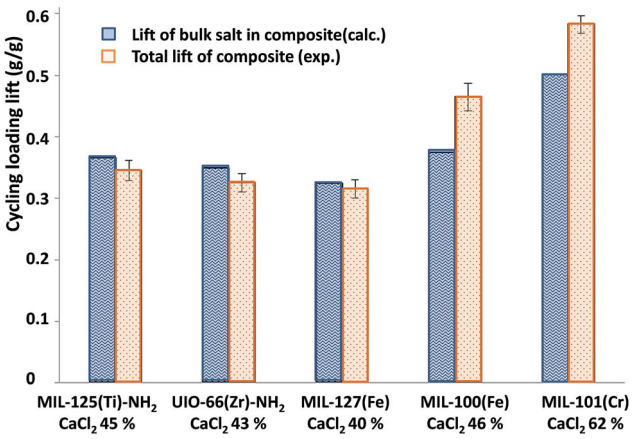

Fig. 4 Cycling loading lift (gram of water per gram of dry composite) of MIL-125(Ti)–NH_2/$CaCl_2$ (45% wt), UiO-66(Zr)–NH_2/$CaCl_2$ (43% wt), MIL-127(Fe)/$CaCl_2$ (40% wt), MIL-100(Fe)/$CaCl_2$ (46 wt%), and MIL-101(Cr)/$CaCl_2$ (62 wt%) and the calculated cycling lift of the salt in the composites. Cycle conditions: adsorption at 30 °C and p = 12.5 mbar, and desorption at 80 °C and p = 12.5 mbar.

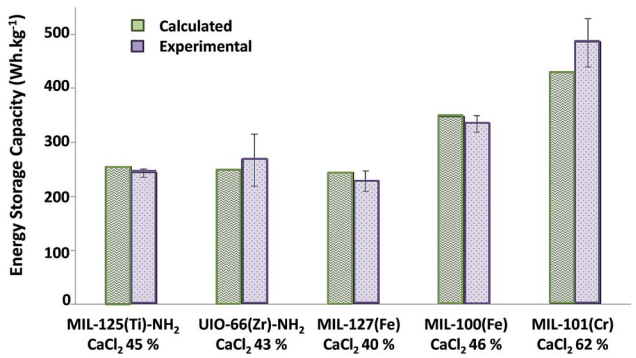

Fig. 5 Calculated and experimental energy storage capacities (W h kg^{-1}) of MIL-125(Ti)–NH_2/$CaCl_2$ (45% wt), UiO-66(Zr)–NH_2/$CaCl_2$ (43% wt), MIL-127(Fe)/$CaCl_2$ (40% wt), MIL-100(Fe)/$CaCl_2$ (46 wt%), and MIL-101(Cr)/$CaCl_2$ (62 wt%).

Published on 18 May 2017. Downloaded on 30/06/2017 09:17:27.

Table 3 The comparison of composites (literature) with MOF based composites (this work) for space heating applications

Matrix	Salt	Salt content (%, wt)	Energy storage capacity (exp.) (W h kg^{-1})	Energy storage density (exp.) (kW h m^{-3})	Adsorption temperature (°C)	Adsorption pressure (mbar)	Desorption temperature (°C)	Ref.
MIL-100(Fe)	$CaCl_2$	46	335[a]/298[b]	208[a]/185[b]	30	12.5	80	This work
MIL-101(Cr)	$CaCl_2$	62	485[a]/446[b]	310[a]/285[b]	30	12.5	80	This work
Comparable desorption temperature conditions								
Silica gel	$CaCl_2$	33.7	132	85	40	17.0	90	65
Silica gel	LiCl	35	254	163	40	17.0	90	66
Silica gel	$CaCl_2$	—	283	—	30	33.9	90	68 and 70
High desorption temperature conditions								
Zeolite 13X	$MgSO_4$	15	180	166	30	15.9	150	65
Attapulgite	$MgSO_4/MgCl_2$	—	397	—	30	31.8	130	61
Aluminosilicate	$CaCl_2$	30	240	—	40	20.0	120	66
FeKIL2 iron silicate	$CaCl_2$	7	155	—	25	12.0	150	64

[a] Energy storage capacity based on the 1st adsorption cycle. [b] Energy storage capacity based on the 10th adsorption cycle.

their corresponding salt composites were prepared under similar conditions (*i.e.* 35 wt% and 40 wt% $CaCl_2$ solution, respectively). It is important to note that in spite of the more favourable cycling conditions for the silica gel based composite in comparison with MIL-100(Fe)/$CaCl_2$ (46 wt%) (*i.e.* higher pressure of adsorption (RH = 80% *versus* 30% at 30 °C) and temperature of regeneration (90 °C *versus* 80 °C)), the storage capacity of the silica gel based composite is lower than that of MIL-100(Fe)/$CaCl_2$ (46 wt%) (283 W h kg^{-1} *versus* 335 W h kg^{-1}).

For regeneration temperatures in the range 120–150 °C, higher energy storage capacity values between 180 and 397 W h kg^{-1} were found for composites based on zeolite 13X, attapulgite, aluminosilicate and iron silicate matrices (Table 3). However, once again, the highest energy storage capacity (397 W h kg^{-1}) reported for composites[64] based on attapulgite and $MgSO_4/MgCl_2$ (mass ratio 20/80) was measured at a higher pressure of adsorption than that used in the present study (31.8 *versus* 12.5 mbar, respectively). These temperature and pressure conditions are nevertheless not adequate for a thermal storage application using solar collectors for heat production and a ground coupled heat exchanger for evaporation and condensation, at least in Northern Europe.

Stability upon adsorption–desorption cycling of MIL-100(Fe)–$CaCl_2$ and MIL-101(Cr)–$CaCl_2$ composites

Finally, in order to evaluate the cycling stability of MIL-100(Fe)/$CaCl_2$ (46 wt%) and MIL-101(Cr)/$CaCl_2$ (62 wt%) composites, these materials were exposed to continuous water adsorption and desorption cycles under representative conditions of seasonal energy storage devices. MIL-100(Fe)/$CaCl_2$ (46 wt%) shows a decrease of about 11% of its initial performance after 11 adsorption–desorption cycles (Fig. 6a) but reaches a steady state after 7 cycles. This results in a slight decrease of its energy storage capacity from 335 to 298 W h kg^{-1} (from 208 to 185 kW h m^{-3}). MIL-101(Cr)/$CaCl_2$ (62 wt%) presents only 8% loss under 10 adsorption–desorption cycles (Fig. 6b) but reaches a steady state after 4 cycles resulting in a reduction of its initial energy storage capacity from 485 to 446 W h kg^{-1} (from 310 to 285 kW h m^{-3}). The stability of MIL-100(Fe)/$CaCl_2$ (46 wt%) and MIL-101(Cr)/$CaCl_2$ (62 wt%) upon cycling was confirmed by collecting SEM, TGA and nitrogen sorption porosimetry measurements

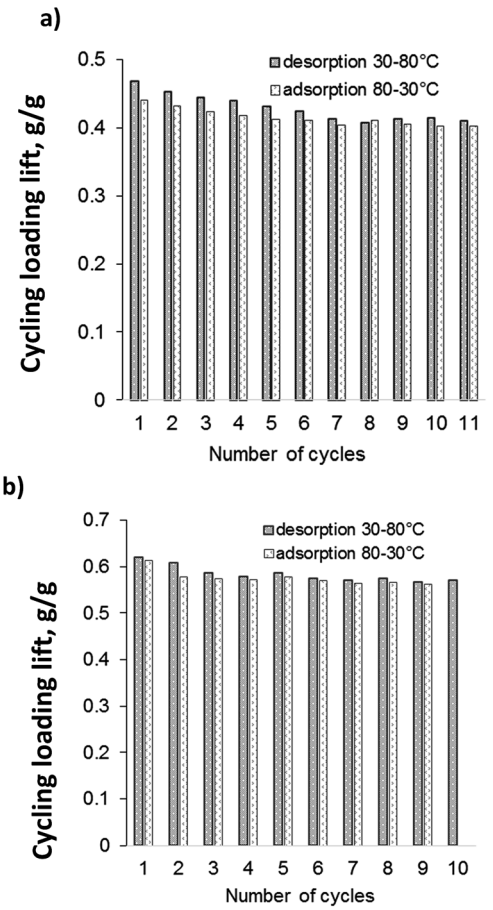

Fig. 6 Stability under numerous adsorption–desorption cycles (p = 12.5 mbar) of (a) MIL-100(Fe)/$CaCl_2$ (46 wt%) and (b) MIL-101(Cr)/$CaCl_2$ (62 wt%).

 This journal is © The Royal Society of Chemistry 2017

Published on 18 May 2017. Downloaded on 30/06/2017 09:17:27.

after ageing the samples for about 18 and 6 months respectively (see Fig. S68–S73†), with no evidence of framework degradation. The high water stability of these composites suggests that these materials pave the way towards the development of new highly efficient water sorbent based processes for heat reallocation.

Conclusions

A series of high loading $CaCl_2$ composites based on robust MOFs bearing various chemical and structural features has been prepared and thoroughly characterised in view of energy reallocation applications such as long term thermal solar energy storage for space heating. Firstly, it has been shown that (i) the increase of salt content in composites significantly enhances the water adsorption capacity of materials and (ii) the hydrophilic character of the MOF–matrix does not improve the overall water uptake due to regeneration or salt hydration limitations. Secondly, the use of amphiphilic MOFs bearing intermediate salt loadings leads to a synergetic effect between water chemisorption of the salt and the physisorption of the MOF, leading to better performances compared with those of the pure MOFs or salt. Finally, the use of mesoporous and amphiphilic robust MOFs is an efficient strategy to achieve higher encapsulation rates and thus, higher loading lifts in comparison with a silica gel matrix. These very promising MOF–salt composites finally exhibit a good cycling performance once a steady state is reached, leading to energy storage densities up to 285 kW h m^{-3} for seasonal storage applications. Although they already outperform most of the other sorbent based composites, one can easily, in the near future, strongly enhance these values through an optimization of the packing density of the composites by using appropriate processing and shaping methods as previously shown.[57] Given the large variety of stable MOF candidates already available, this finally paves the way for the design of advanced composites based on new MOF matrices for energy reallocation applications.

Acknowledgements

The authors acknowledge the financial support from the European Community within the 7th Framework Program (FP7) under grant agreement No. 295775 (Project SoTherCo, website: http://www.sotherco.eu/). The authors are thankful to Dr Daniel Lager and Dr Wolfgang Hohenauer from the Austrian Institute of Technology (AIT) for statistics on calorimetric measurements.

Notes and references

1 M. F. de Lange, K. J. F. M. Verouden, T. J. H. Vlugt, J. Gascon and F. Kapteijn, *Chem. Rev.*, 2015, **115**, 12205.
2 Y. I. Aristov, *Appl. Therm. Eng.*, 2013, **50**, 1610.
3 F. Jeremias, D. Fröhlich, C. Janiak and S. K. Henninger, *New J. Chem.*, 2014, **38**, 1846.
4 K. E. N'Tsoukpoe, H. Liu, N. Le Pierrès and L. Luo, *Renewable Sustainable Energy Rev.*, 2009, **13**, 2385.
5 A. Solé, I. Martorell and L. F. Cabeza, *Renewable Sustainable Energy Rev.*, 2015, **47**, 386.
6 D. Aydin, S. P. Casey and S. Riffat, *Renewable Sustainable Energy Rev.*, 2015, **41**, 356.
7 S. K. Henninger, S.-J. Ernst, L. Gordeeva, P. Bendix, D. Fröhlich, A. D. Grekova, L. Bonaccorsi, Y. Aristov and J. Jaenchen, *Renewable Energy*, 2017, **110**, 59–68.
8 B. B. Saha, A. Chakraborty, S. Koyama and Y. I. Aristov, *Int. J. Heat Mass Transfer*, 2009, **52**, 516.
9 S. Shimooka, K. Oshima, H. Hidaka, T. Takewaki, H. Kakiuchi, A. Kodama, M. Kubota and H. Matsuda, *J. Chem. Eng. Jpn.*, 2007, **40**, 1330.
10 A. Krajnc, J. Varlec, M. Mazaj, A. Ristić, N. Z. Logar and G. Mali, *Adv. Energy Mater.*, 2017, 1601815.
11 A. Ristić, N. Z. Logar, S. K. Henninger and V. Kaučič, *Adv. Funct. Mater.*, 2012, **22**, 1952.
12 L. F. Cabeza, A. Solé and C. Barreneche, *Renewable Energy*, 2017, **110**, 3–39.
13 F. Kuznik, K. Johannes and C. Obrecht, *Energy Build*, 2015, **106**, 183.
14 A. Jabbari-Hichri, S. Bennici and A. Auroux, *Sol. Energy Mater. Sol. Cells*, 2015, **140**, 351.
15 Y. I. Aristov, M. M. Tokarev, G. Cacciola and G. Restuccia, *React. Kinet. Catal. Lett.*, 1996, **59**, 325.
16 Y. I. Aristov, M. M. Tokarev, G. Restuccia and G. Cacciola, *React. Kinet. Catal. Lett.*, 1996, **59**, 335.
17 E. Levitskij, *Sol. Energy Mater. Sol. Cells*, 1996, **44**, 219.
18 Y. I. Aristov, G. Di Marco, M. M. Tokarev and N. V. Parmon, *React. Kinet. Catal. Lett.*, 1997, **61**, 147.
19 Y. I. Aristov, *J. Chem. Eng. Jpn.*, 2007, **40**, 1242.
20 I. A. Simonova and Y. I. Aristov, *Russ. J. Phys. Chem.*, 2005, **79**, 1307.
21 I. A. Simonova, A. Freni, G. Restuccia and Y. I. Aristov, *Microporous Mesoporous Mater.*, 2009, **122**, 223.
22 E. Courbon, P. D'Ans, A. Permyakova, O. Skrylnyk, N. Steunou, M. Degrez and M. Frère, *Appl. Energy*, 2017, **190**, 1184.
23 Themed issue, *Chem. Soc. Rev.*, 2014, **43**, 5403.
24 (*a*) L. J. Murray, M. Dincă and J. R. Long, *Chem. Soc. Rev.*, 2009, **38**, 1294; (*b*) P. Nugent, Y. Belmabkhout, S. D. Burd, A. J. Cairns, R. Luebke, K. Forrest, T. Pham, S. Ma, B. Space, L. Wojtas, M. Eddaoudi and M. J. Zaworotko, *Nature*, 2013, **495**, 80.
25 Q. Yang, S. Vaesen, F. Ragon, A. D. Wiersum, D. Wu, A. Lago, T. Devic, C. Martineau, F. Taulelle, P. L. Llewellyn, H. Jobic, C. Zhong, C. Serre, G. De Weireld and G. Maurin, *Angew. Chem., Int. Ed.*, 2013, **52**, 10316.
26 J. Lee, O. K. Farha, J. Roberts, K. A. Scheidt, S. T. Nguyen and J. T. Hupp, *Chem. Soc. Rev.*, 2009, **38**, 1450.
27 P. Horcajada, S. Surblé, C. Serre, D.-Y. Hong, Y.-K. Seo, J.-S. Chang, J.-M. Grenèche, I. Margiolaki and G. Férey, *Chem. Commun.*, 2007, 2820.
28 A. Corma, H. García and F. X. Llabrés i Xamena, *Chem. Rev.*, 2010, **110**, 4606.
29 J. Gascon, A. Corma, F. Kapteijn and F. X. Llabrés i Xamena, *ACS Catal.*, 2014, **4**, 361.
30 P. Horcajada, T. Chalati, C. Serre, B. Gillet, C. Sebrie, T. Baati, J. F. Eubank, D. Heurtaux, P. Clayette, C. Kreuz, J.-S. Chang, Y. K. Hwang, V. Marsaud, P.-N. Bories,

Published on 18 May 2017. Downloaded on 30/06/2017 09:17:27.

L. Cynober, S. Gil, G. Férey, P. Couvreur and R. Gref, *Nat. Mater.*, 2010, **9**, 172.
31 P. Horcajada, R. Gref, T. Baati, P. K. Allan, G. Maurin, P. Couvreur, G. Férey, R. E. Morris and C. Serre, *Chem. Rev.*, 2012, **112**, 1232.
32 M. Meilikhov, S. Furukawa, K. Hirai, R. A. Fischer and S. Kitagawa, *Angew. Chem., Int. Ed.*, 2013, **52**, 341.
33 L. E. Kreno, K. Leong, O. K. Farha, M. Allendorf, R. P. Van Duyne and J. T. Hupp, *Chem. Rev.*, 2012, **112**, 1105.
34 S. Patra, T. Hidalgo Crespo, A. Permyakova, C. Sicard, C. Serre, A. Chaussé, N. Steunou and L. Legrand, *J. Mater. Chem. B*, 2015, **3**, 8983.
35 F. Jeremias, V. Lozan, S. K. Henninger and C. Janiak, *Dalton Trans.*, 2013, **42**, 15967.
36 F. Jeremias, A. Khutia, S. K. Henninger and C. Janiak, *J. Mater. Chem.*, 2012, **22**, 10148.
37 J. Canivet, A. Fateeva, Y. Guo, B. Coasne and D. Farrusseng, *Chem. Soc. Rev.*, 2014, **43**, 5594.
38 Y.-K. Seo, J. W. Yoon, J. S. Lee, Y. K. Hwang, C.-H. Jun, J.-S. Chang, S. Wuttke, P. Bazin, A. Vimont, M. Daturi, S. Bourrelly, P. L. Llewellyn, P. Horcajada, C. Serre and G. Férey, *Adv. Mater.*, 2012, **24**, 806.
39 H. Furukawa, F. Gándara, Y.-B. Zhang, J. Jiang, W. L. Queen, M. R. Hudson and O. M. Yaghi, *J. Am. Chem. Soc.*, 2014, **136**, 4369.
40 E. Elsayed, R. AL-Dadah, S. Mahmoud, A. Elsayed and P. A. Anderson, *Appl. Therm. Eng.*, 2016, **99**, 802.
41 H. Reinsch, M. A. van der Veen, B. Gil, B. Marszalek, T. Verbiest, D. de Vos and N. Stock, *Chem. Mater.*, 2013, **25**, 17.
42 N. Reimer, B. Bueken, S. Leubner, C. Seidler, M. Wark, D. De Vos and N. Stock, *Chem.–Eur. J.*, 2015, **21**, 12517.
43 D. Fröhlich, E. Pantatosaki, P. D. Kolokathis, K. Markey, H. Reinsch, M. Baumgartner, M. A. van der Veen, D. E. De Vos, N. Stock, G. K. Papadopoulos, S. K. Henninger and C. Janiak, *J. Mater. Chem. A*, 2016, **4**, 11859.
44 A. Cadiau, J. S. Lee, D. Damasceno Borges, P. Fabry, T. Devic, M. T. Wharmby, C. Martineau, D. Foucher, F. Taulelle, C.-H. Jun, Y. K. Hwang, N. Stock, M. F. De Lange, F. Kapteijn, J. Gascon, G. Maurin, J.-S. Chang and C. Serre, *Adv. Mater.*, 2015, **27**, 4775.
45 F. Jeremias, A. Khutia, S. K. Henninger and C. Janiak, *J. Mater. Chem.*, 2012, **22**, 10148.
46 M. F. De Lange, J.-J. Gutierrez-Sevillano, S. Hamad, T. J. H. Vlugt, S. Calero, J. Gascon and F. Kapteijn, *J. Phys. Chem. C*, 2013, **117**, 7613.
47 G. Akiyama, R. Matsuda, H. Sato, A. Hori, M. Takata and S. Kitagawa, *Microporous Mesoporous Mater.*, 2012, **157**, 89.
48 S.-I. Kim, T.-U. Yoon, M.-B. Kim, S.-J. Lee, Y. K. Hwang, J.-S. Chang, H.-J. Kim, H.-N. Lee, U.-H. Lee and Y.-S. Bae, *Chem. Eng. J.*, 2016, **286**, 467.
49 N. Ko, P. G. Choi, J. Hong, M. Yeo, S. Sung, K. E. Cordova, H. J. Park, J. K. Yang and J. Kim, *J. Mater. Chem. A*, 2015, **3**, 2057.
50 A. Permyakova, O. Skrylnyk, E. Courbon, M. Affram, S. Wang, U.-H. Lee, A. H. Valekar, F. Nouar, G. Mouchaham, T. Devic, G. De Weireld, J.-S. Chang, N. Steunou, M. Frère and C. Serre, *ChemSusChem*, 2017, **10**, 1419–1426.
51 (*a*) H. Chevreau, A. Permyakova, F. Nouar, P. Fabry, C. Livage, F. Ragon, A. Garcia-Marquez, T. Devic, N. Steunou, C. Serre and P. Horcajada, *CrystEngComm*, 2016, **18**, 4094; (*b*) Y. Belmabkhout, R. S. Pillai, D. Alezi, O. Shekhah, P. M. Bhatt, Z. Chen, K. Adil, S. Vaesen, G. De Weireld, M. Pang, M. Suetin, A. J. Cairns, V. Solovyeva, A. Shkurenko, O. El Tall, G. Maurin and M. Eddaoudi, *J. Mater. Chem. A*, 2017, **5**, 3293.
52 G. Férey, C. Mellot-Draznieks, C. Serre, F. Millange, J. Dutour, S. Surblé and I. Margiolaki, *Science*, 2005, **309**, 2040.
53 J. H. Cavka, S. Jakobsen, U. Olsbye, N. Guillou, C. Lamberti, S. Bordiga and K. P. Lillerud, *J. Am. Chem. Soc.*, 2008, **130**, 13850.
54 M. Kandiah, M. H. Nilsen, S. Usseglio, S. Jakobsen, U. Olsbye, M. Tilset, C. Larabi, E. A. Quadrelli, F. Bonino and K. P. Lillerud, *Chem. Mater.*, 2010, **22**, 6632.
55 Y. Fu, D. Sun, Y. Chen, R. Huang, Z. Ding, X. Fu and Z. Li, *Angew. Chem., Int. Ed.*, 2012, **51**, 3364.
56 G. E. Cmarik, M. Kim, S. M. Cohen and K. S. Walton, *Langmuir*, 2012, **28**, 15606.
57 L. Garzón-Tovar, J. Pérez-Carvajal, I. Imaz and D. Maspoch, *Adv. Funct. Mater.*, 2017, 1606424.
58 A. Khutia, H. U. Rammelberg, T. Schmidt, S. Henninger and C. Janiak, *Chem. Mater.*, 2013, **25**, 790.
59 P.-J. Kim, Y.-W. You, H. Park, J.-S. Chang, Y.-S. Bae, C.-H. Lee and J.-K. Suh, *Chem. Eng. J.*, 2015, **262**, 683.
60 R. Canioni, C. Roch-Marchal, F. Sécheresse, P. Horcajada, C. Serre, M. Hardi-Dan, G. Férey, J.-M. Grenèche, F. Lefebvre, J.-S. Chang, Y.-K. Hwang, O. Lebedev, S. Turner and G. Van Tendeloo, *J. Mater. Chem.*, 2011, **21**, 1226.
61 (*a*) H. Wu, Y. S. Chua, V. Krungleviciute, M. Tyagi, P. Chen, T. Yildirim and W. Zhou, *J. Am. Chem. Soc.*, 2013, **135**, 10525; (*b*) G. C. Shearer, S. Chavan, J. Ethiraj, J. G. Vitillo, S. Svelle, U. Olsbye, C. Lamberti, S. Bordiga and K. P. Lillerud, *Chem. Mater.*, 2014, **26**, 4068.
62 I. Glaznev, I. Ponomarenko, S. Kirik and Y. Aristov, *Int. J. Refrig.*, 2011, **34**, 1244.
63 Y. I. Aristov, G. Restuccia, G. Cacciola and V. N. Parmon, *Appl. Therm. Eng.*, 2002, **22**, 191.
64 K. Posern and C. Kaps, *Thermochim. Acta*, 2010, **502**, 73.
65 C. Bales, P. Gantenbein, A. Hauer, H.-M. Henning, D. Jaenig, H. Kerskes, T. Núñez and K. Visscher, *Rep. IEA Sol. Heat. Cool. Program.*, 2005, p. 32.
66 N. Yu, R. Z. Wang, Z. S. Lu and L. W. Wang, *Chem. Eng. Sci.*, 2014, **111**, 73.
67 A. Ristić, D. Maučec, S. K. Henninger and V. Kaučič, *Microporous Mesoporous Mater.*, 2012, **164**, 266.
68 S. Hongois, F. Kuznik, P. Stevens and J.-J. Roux, *Sol. Energy Mater. Sol. Cells*, 2011, **95**, 1831.
69 J. Jänchen, D. Ackermann, H. Stach and W. Brösicke, *Sol. Energy*, 2004, **76**, 339.
70 H. Wu, S. Wang and D. Zhu, *Sol. Energy*, 2007, **81**, 864.

 This journal is © The Royal Society of Chemistry 2017